IEEE Robotics and Automation Letters (RAL) paper presented at the
2018 IEEE International Conference on Robotics and Automation (ICRA)
May 21-25, 2018, Brisbane, Australia

Mechanical Rubbing of Blood Clots using Helical Robots under Ultrasound Guidance

Islam S. M. Khalil, Dalia Mahdy, Ahmed El Sharkawy, Ramez R. Moustafa,
Ahmet Fatih Tabak, Mohamed E. Mitwally, Sarah Hesham, Nabila Hamdi, Anke Klingner, and Metin Sitti

***Abstract*— A simple way to mitigate the potential negative side-effects associated with chemical lysis of a blood clot is to tear its fibrin network via mechanical rubbing using a helical robot. Here we achieve mechanical rubbing of blood clots under ultrasound guidance and using external magnetic actuation. Position of the helical robot is determined using ultrasound feedback and used to control its motion towards the clot, whereas the volume of the clots is estimated simultaneously using visual feedback. We characterize the shear modulus and ultimate shear strength of the blood clots to predict their removal rate during rubbing. Our *in vitro* experiments show the ability to move the helical robot controllably towards clots using ultrasound feedback with average and maximum errors of 0.84 ± 0.41 mm and 2.15 mm, respectively, and achieve removal rate of -0.614 ± 0.303 mm^3/min at room temperature (25°C) and -0.482 ± 0.23 mm^3/min at body temperature (37°C), under the influence or two rotating dipole fields at frequency of 35 Hz. We also validate the effectiveness of mechanical rubbing by measuring the number of red blood cells and platelets past the clot. Our measurements show that rubbing achieves cell count of $46 \pm 10.9 \times 10^4$, whereas the count in the absence of rubbing is $2 \pm 1.41 \times 10^4$ cell/ml, after 40 minutes.**

I. Introduction

Blood clots can occur and travel to deep seated regions of the human body and may cause significant problems as blood flow past the clot is decreased. Fibrinolytics and anticoagulant drugs have long been used to treat and prevent blood clots within blood vessels. However, special medical precautions and tests are necessary to avoid several side-effects such as excessive bleeding. A simple way to mitigate these side-effects is through the localization of the drug [1] or interaction with the clot via external magnetic field actuation of a microrobot. Vonthron *et al.* have demonstrated steering, localization, and control of microrobots and microdevices using a clinical magnetic resonance imaging system [2]. Servant *et al.* have controlled a swarm of functionalized artificial bacterial flagella *in vivo* using rotating magnetic field in millitesla range, and using feedback of an optical fluorescence imaging system [3]. Felfoul *et al.* have also transported drug-loaded nanoliposomes into hypoxic regions of the tumour using the magneto-aerotactic migration behaviour of *Magnetococcus marinus* strain MC-1 [4], and demonstrated improvement in the therapeutic index during targeted drug delivery. Srivastava *et al.* have also shown dual-functionality of creating cellular incision together with site-directed drug delivery using biotubes [5]. Very recently, drug-loaded magnesium micromotors have been used to demonstrate *in vivo* antibiotic delivery in the gastric media of a mouse model [6]. The versatility of microrobots (driven by magnetic [7], [8], bubble [9], ultrasound [10], electric [11], and electrophoretic propulsion [12]) has proven to be unlimited and offer promise for diverse biomedical applications such as drug delivery [13], diagnostics [14], cell manipulation and sorting [15], biopsy, and precision nanosurgery.

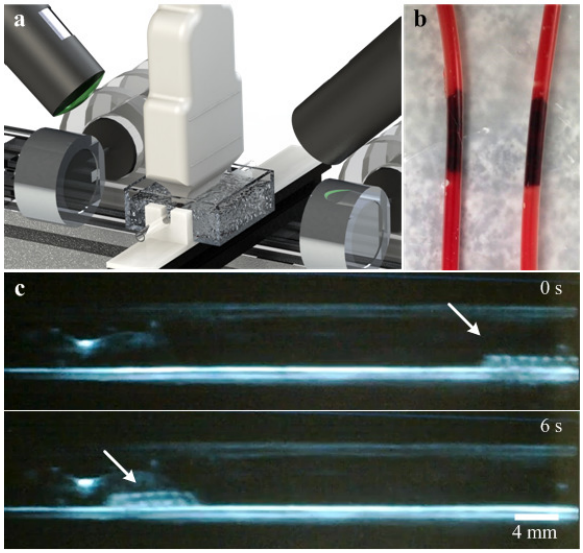

Fig. 1. Rubbing against a blood clot is achieved using a helical robot driven by two synchronized rotating dipole fields. (a) The robot is tracked using an ultrasound imaging modality (NOCTN340, HD5 Diagnostic Ultrasound System, Philips and Neusoft Medical Systems, Amsterdam, The Netherlands), whereas the volume of the clot is determined using 2 cameras throughout the rubbing. (b) Clots are inserted into catheter segments filled with phosphate buffered saline. The segment is contained inside a gelatin container to achieve air-free coupling between the transducer and the catheter segment. (c) The helical robot (white arrow) swims controllably towards the clot at average speed of 4 mm/s ($\omega = 35$ Hz), and starts rubbing at time $t = 6$ s.

Here, we focus on a potential medical application (removal of blood clots) of helical robots driven by rotating magnetic fields (Fig. 1). In our previous work [16], an optimal rubbing frequency of blood clots is determined using a hydrodynamic model based on the resistive-force theory (RFT). In this

This work was supported by the DAAD-BMBF funding project and the Science and Technology Development Fund in Egypt (No. 23016).

I. S. M. Khalil, D. Mahdy, A. El Sharkawy, M. E. Mitwally, S. Hesham, N. Hamdi, A. Klingner are with the German University in Cairo, Egypt (e-mail: islam.shoukry@guc.edu.eg).

A. F. Tabak and M. Sitti are with the Physical Intelligence Department, Max Planck Institute for Intelligent Systems, Stuttgart, Germany.

R. R. Moustafa is with the Department of Neurology, Ain Shams University, Egypt.

work, we achieve the following: (1) characterization of the mechanical properties of blood clots using rheology test at room and body temperatures (properties of blood clots are poorly known and its essential to provide our RFT-based model with the ultimate shear strength to predict the removal rate of the clot); (2) design of a closed-loop control system based on ultrasound feedback; (3) validation of the effectiveness of the helical robot via removal rate and cell count throughout the interaction between the robot and the clot. The remainder of this paper is organized as follows: Section II provides characterization of the blood clots. A hydrodynamic model of the rubbing behaviour is also presented to calculate the removal rate of clots during rubbing. Section III presents localization of the helical robot using ultrasound feedback, closed-loop control of the helical robot, and *in vitro* rubbing of blood clots under ultrasound guidance. The effect of body temperature on the removal rate of blood clots and the influence of the mechanical rubbing on the red blood cells (RBCs) and platelets past the clot is also analyzed in Section III. A discussion pertaining to the difference between our *in vitro* model and *in vivo* conditions is presented in Section IV. Finally, Section V concludes and provides directions for future work.

II. Modeling and Characterization of Rubbing

Ischemic tissue deprived of blood will not survive indefinitely and thus the relation between the clot removal rate and the control inputs must be well understood to minimize the rubbing time. We provide a physical picture of the rubbing behaviour using our RFT-based hydrodynamic model to relate the removal rate to the control and robot parameters.

A. Mechanical Rubbing of Blood Clots

Following our previous work [16], we model the interaction between the tip of the helical robot and the three-dimensional network of the fibrin fibers of the clot using conservation of energy and momentum. The work done by the tip of the rotating tail is equal to the work done by the removed material. Therefore, we approximate the net torque required to remove an infinitesimal depth (δ_{bc}) of the clot using

$$(\mid T_{\mathrm{m},x} \mid - \mid T_{\mathrm{d},x} \mid)\,\omega \approx 0.25\pi\tau r_{\mathrm{h}}\omega\delta_{\mathrm{bc}}^2, \qquad (1)$$

where $T_{\mathrm{m},x}$ and $T_{\mathrm{d},x}$ are the magnetic and drag torque exerted on the helical robot during rubbing with respect to the long axis of the helix. Further, ω is the angular velocity of the robot with respect to the helix axis, and τ and r_{h} are the ultimate shear strength of the clot and the radius of the helix, respectively. We consider the ultimate shear strength since the basic action of the robot is to remove parts of the clot by rubbing or shearing a layer of its material with respect to another underneath. In (1), the magnetic torque is generated using two synchronized rotating dipole fields. These dipole fields ($\mathbf{B}_1$ and $\mathbf{B}_2$) exert the following magnetic torque ($\mathbf{T}_{\mathrm{m}}$) on the magnetic dipole moment ($\mathbf{m}$) of the helical robot:

$$\begin{pmatrix}\mathbf{F}_{\mathrm{m}}\\ \mathbf{T}_{\mathrm{m}}\end{pmatrix} = \begin{pmatrix}(\mathbf{m}\cdot\nabla)(\mathbf{R}_1\mathbf{B}_1+\mathbf{R}_2\mathbf{B}_2)\\ \mathbf{m}\times(\mathbf{R}_1\mathbf{B}_1+\mathbf{R}_2\mathbf{B}_2)\end{pmatrix}, \qquad (2)$$

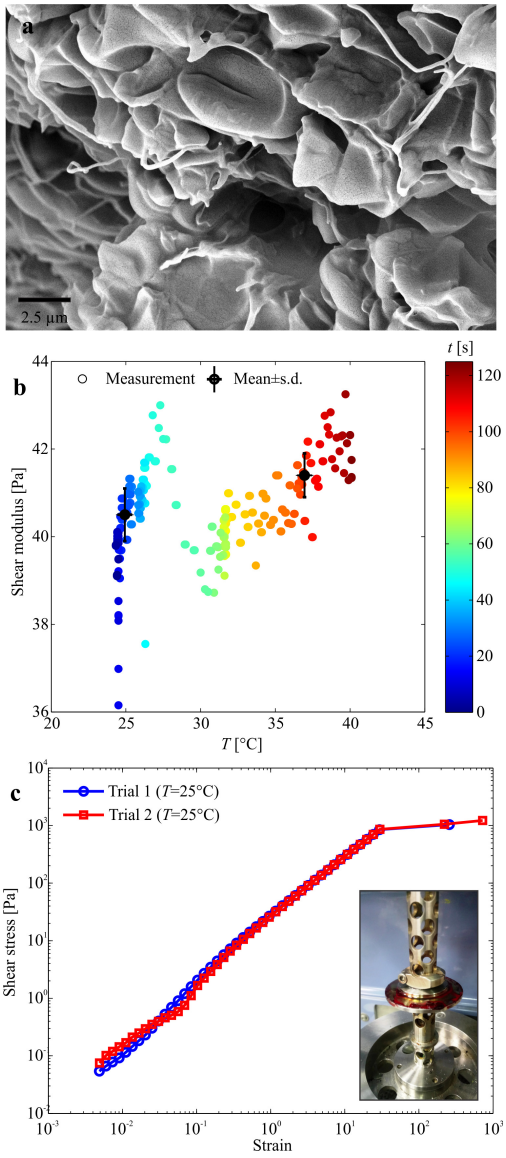

Fig. 2. Morphology and mechanical properties of the blood clots are characterized using scanning electron microscopy (SEM) imaging and rheology test. (a) An SEM image shows blood cells entrapped inside the fibrin network of the clot. (b) Rheology test is done using a Bohlin Gemini instrument (Malvern Instruments, U.K.). The shear modulus of 1-hour-old samples is 40.5 ± 0.6 Pa and 41.4 ± 0.5 Pa at 25 ± 0.5°C and body temperature (37 ± 0.5°C), respectively. (c) The shear stress-strain diagram of the clots indicates that the ultimate shear strength (τ) is 1 kPa. The inset shows a 1-hour-old clot samples fixed between the lower and upper plates.

where $\mathbf{F}_{\mathrm{m}}$ is the magnetic force. Further, $\mathbf{R}_1$ and $\mathbf{R}_2$ are rotation matrices from frames of the first and second rotating dipole fields to the frame of reference of the robot, respectively. The drag torque ($\mathbf{T}_{\mathrm{d}}$) given in (1) is calculated using

$$\begin{pmatrix}\mathbf{F}_{\mathrm{d}}\\ \mathbf{T}_{\mathrm{d}}\end{pmatrix} = \left(\int_l \begin{bmatrix}\mathbf{RCR}^{\mathrm{T}} & -\mathbf{RCR}^{\mathrm{T}}\mathbf{S}\\ \mathbf{SRCR}^{\mathrm{T}} & -\mathbf{SRCR}^{\mathrm{T}}\mathbf{S}\end{bmatrix} \mathrm{d}l + \begin{bmatrix}\mathbf{R}_{\mathrm{ch}}\mathbf{D}\mathbf{R}_{\mathrm{ch}}^{\mathrm{T}} & -\mathbf{R}_{\mathrm{ch}}\mathbf{D}\mathbf{R}_{\mathrm{ch}}^{\mathrm{T}}\mathbf{S}\\ \mathbf{S}\mathbf{R}_{\mathrm{ch}}\mathbf{D}\mathbf{R}_{\mathrm{ch}}^{\mathrm{T}} & \mathbf{E}\end{bmatrix}\right)\begin{pmatrix}\mathbf{U}+\mathbf{U}_{\mathrm{ch}}\\ \boldsymbol{\Omega}\end{pmatrix}, \qquad (3)$$

where $\mathbf{F}_{\mathrm{d}}$ is the drag force imparted to the fluid by the helical robot. Further, $\mathbf{U}$ and $\mathbf{\Omega}$ are the linear and angular velocities of the helical robot, respectively, and $\mathbf{U}_{\mathrm{ch}}$ is the flow inside the catheter segment that contains the clot. Further, $\mathbf{R}$ is the rotation matrix between local Frenet-Serret frames and the reference frame of the robot, and $\mathbf{C}$ is the resistance coefficient matrix. $\mathbf{R}_{\mathrm{ch}}$ is a projection matrix of the cylindrical coordinates of the channel to the Cartesian coordinates residing on the center of mass of the robot, and $\mathbf{S}$ signifies local cross products. Matrix $\mathbf{D}$ provides the fluid resistance coefficients of the magnetic head for the translational rigid-body motion and $\mathbf{E}$ provides the fluid resistance coefficients of the head for the rotational rigid-body motion. In order to predict the rubbing behaviour between the helical robot and the fibrin network of the clot using (1)-(3), we characterize the mechanical properties of the blood clot to estimate the material removal rate during rubbing.

B. Characterization of Blood Clots

Blood clots are prepared based on the protocol proposed by Hoffmann and Gill [17] and approved by the local Institutional Review Board. Donors' written informed consent are obtained. Blood is drawn from four healthy donors between the ages of 25 and 28. Fig. 2 shows a scanning electron microscopy (SEM) image of a blood clot sample. It indicates that blood cells are entrapped inside the fibrin network of the clot. Cines *et al.* have also observed similar morphology of contracted blood cells inside the clots [18]. Therefore, their structure is similar to clots inside the human circulatory system. Characterization using rheology test, control, and rubbing are done using 1-hour-old blood clot samples. The clots are placed between a lower plate with diameter of 40 mm and an upper plate with diameter of 25 mm. The clots are surrounded by oil with viscosity of 0.06 Pas to avoid drying and denaturation of the samples. The gap between the plates is 1.569 mm and oscillatory shear with maximum shear stress of 0.1 Pa is applied at frequency of 1 Hz. At room temperature (25°C) and body temperature (37°C), shear modulus is measured to be 40.5 ± 0.6 Pa and 41.4 ± 0.5 Pa, respectively, as shown in Fig. 2(b). Fig. 2(c) shows the stress-strain relation of the blood clots for two representative trials. This characterization experiment indicates that the ultimate shear strength of 1-hour-old blood clots is approximately 1 kPa. This value is used in (1) to predict the theoretical removal rate of the clot during rubbing.

The rubbing behaviour between the tip of the helical robot and the fibrin network of a clot is shown in Fig. 3. This trajectory is calculated for a 4-mm-long helical robot with diameter of 346 μm. The helix angle is 45° and the wire diameter is 100 μm. We allow the helical robot to rotate at angular frequency (ω) of 35 Hz with respect to its long axis in phosphate buffered saline (PBS) with viscosity of 0.8882 Pa.s. Although the rheology test (Fig. 2) indicates that the clot is relatively soft, our simulation result show that the tip of the helical robot does not drill through the fibrin network upon contact. For approximately 25 minutes, the tip of the helical robot grinds the face of the clot and penetration

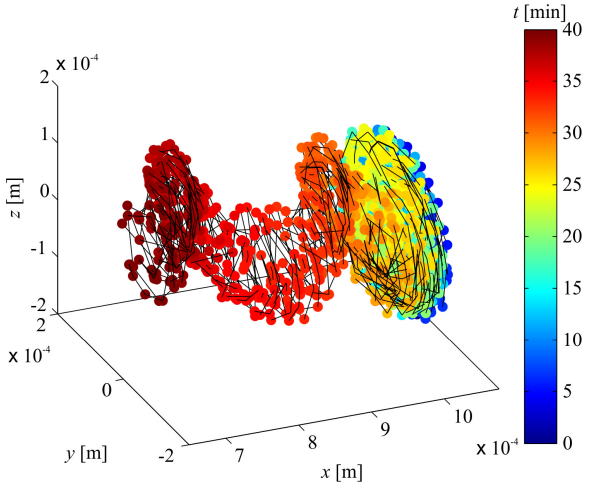

Fig. 3. Simulation of the rubbing behaviour between the helical robot and the fibrin network of the blood clot is demonstrated for 40 minutes. The trajectory of the robot is calculated using (1)-(3) for a 4-mm-long helical robot with diameter of 346 μm, and a 7.5-mm-long blood clot with diameter of 4 mm in a medium with viscosity of 0.8882 Pa.s and clot with ultimate shear strength of 1000 Pa. The helical robot achieves a penetration with depth of 0.1 mm after 25 minutes of rubbing at ω=35 Hz. At approximately t=27 min, the helical robot follows a helical trajectory and achieves penetration with depth of 0.4 mm inside the clot.

of approximately 0.1 mm is achieved. We observe that the tip of the robot follows a helical trajectory inside the clot at time $t = 28$ minutes. After 40 minutes, the tip of the robot achieves a depth of 0.4 mm (10% of the clot diameter) inside the clot while rotating. Therefore, the simulation result in Fig. 3 provides two distinct responses for the interaction between the helical robot and the clot. First, the tip grinds the face of the clot and achieves relatively low penetration. Second, the helical robot drills through the clot with a helical trajectory and relatively greater depth and achieves removal rate of -0.5992 mm^3/min, at $\omega = 35$ Hz. Our simulation results show that the tip of the helical robot cannot penetrate the blood clot upon immediate contact with its surface. The interaction between the clot and the tip of the helical tail is modeled via a spring force [16], and as a consequence, the robot is pushed back upon contact with the surface of the clot in any arbitrary direction ($t < 28$ min). Once a groove into the network of the blood clot is created, the robot drills through the clot while rubbing its fibrin network ($28 < t < 40$ min). Therefore, material removal rate is increased owing to this action, as shown in Fig. 3. This prediction can be further improved by numerically introducing smaller slices and segments along the surface to represent local material removal with relatively higher accuracy.

III. Localization, Control, and Rubbing of Blood Clots using Ultrasound Feedback

In vitro rubbing of blood clots is achieved using a permanent magnet-based robotic system and ultrasound feedback.

A. System Description

The permanent magnet-based robotic system consists of two rotating dipole fields to exert magnetic torque on the

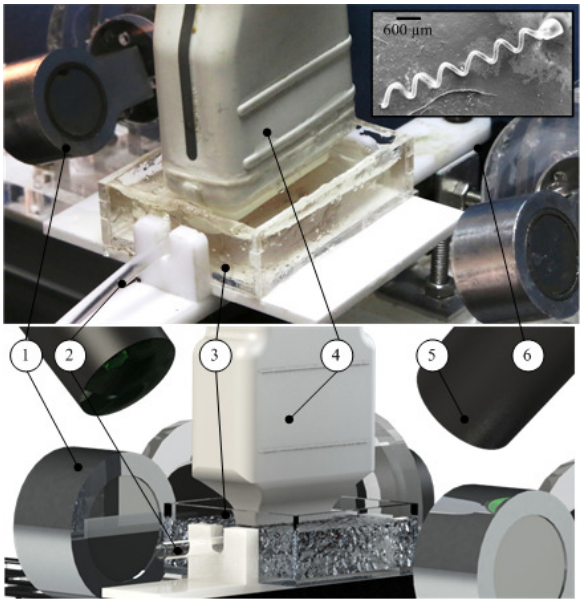

Fig. 4. Mechanical rubbing of a blood clot is achieved using a helical robot under the influence of rotating dipole fields ①. The blood clot (1-hour-old) is contained inside a catheter segment ② and the helical robot achieves helical propulsion in phosphate buffered saline. The catheter segment is contained inside a reservoir ③ filled with gelatin. Position of the helical robot (inset) is detected using an ultrasound probe ④ (L12-3 broadband linear array transducer, Philips and Neusoft Medical Systems, Amsterdam, The Netherlands), whereas the size of the clot is measured using camera ⑤ feedback. The helical robot ⑥ has length of 4 mm and diameter of 346 μm.

magnetic dipole of the helical robot (Fig. 4). The helical robot is fabricated using an aluminum spring with diameter and pitch of 346 μm and 581 μm, respectively. The spring is attached to a cylindrical NdFeB magnet with axial magnetization oriented perpendicular to the spring axis and magnetic flux density (B_r) of 1420 mT. Therefore, its magnetization is approximated using the volume integral as $\mid \mathbf{m} \mid = \frac{1}{\mu_0}\int B_\mathrm{r}\mathrm{d}v$, resulting in $\mid \mathbf{m} \mid$=1.72$\times 10^{-4}$ A.m^2, where μ_0 is the permeability of free space. The resultant magnetic field at the position of the helical robot is 5.5 mT. Rotation of the permanent magnets is achieved via two synchronized motors (2322 980, Maxon Motor, Sachseln, Switzerland). The two rotating permanent magnets exert pure magnetic torque only when the dipole of the helical robot is positioned in the middle of their common centers [19]. Air-free coupling between the transducer and the blood clot is achieved using gelatin. The gelatin is prepared and contained inside a rectangular reservoir with length, width, and depth of 6 cm, 4.5 cm, and 1.5 cm, respectively. This reservoir hosts a polyvinyl chloride catheter segment filled with PBS and 1-hour-old blood clot sample. The catheter segment is connected to a dual syringe pump (Genie Plus, GT-4201D-12, Kent Scientific, Connecticut, USA) to induce flow rate of 10 ml/hr against the direction of the swimming helical robot. The PBS and blood mixture past the clot and the helical robot is contained inside a reservoir and collected each 5 minutes. This mixture is analyzed using hemocytometer for cell count.

B. Localization of the Robot using Ultrasound Feedback

An ultrasound system (HD 5 Diagnostic Ultrasound System, Philips and Neusoft Medical Systems, Amsterdam, The Netherlands) with maximum depth of field of 16 cm is integrated to our permanent magnet-based robotic system to visualize the helical robot. The transducer (NOCTN340, Philips and Neusoft Medical Systems, Amsterdam, The Netherlands) of the system is mounted on the surface of the gelatin at hight of 7.5 mm from the catheter segment, as shown in Fig. 4. The depth of the catheter segment can be increased to localize the robot at relatively deeper distances from the surface (Fig. 5(a)). However, the wavelength and frequency of the propagating ultrasound waves are inversely proportional. Therefore, high-frequency ultrasound waves generate images with higher resolution and can only be used to localize superficial structures. The high-frequency ultrasound waves are attenuated as the depth increases and therefore low-frequency ultrasound waves are more suitable for relatively deep clots. The ultrasound system is set to motion mode (*M-mode*) to display a sequence of rapidly acquired scans during helical propulsion inside the catheter segment. The thermal index score and the mechanical index are 0.2 and 0.9, respectively. All scans are acquired for gain setting, frequency, and depth of 43, 10 MHz, and 3 cm, respectively. Figs. 5(b-i) show the implemented steps of image processing to localize the helical robot.

The feedback provided by the ultrasound system is used to track the helical robot. However, the level of echogenicity of our blood clots does not enable visualization using ultrasound feedback. We attribute the low echogenicity of the clots to their age. 1-hour-old blood clot samples are used in our trials as its essential to achieve early intervention in the beginning of the clot formation. In addition, the rubbing time is limited to 40 minutes as its essential to remove the clot within a biologically meaningful time. Therefore, two cameras are used to determine the size of the blood clot during rubbing. The two cameras are oriented with 45° with respect to the horizontal plane and have 90° with respect to each other. The ultrasound feedback is used in the design of a closed-loop motion control system for the helical robot, whereas the camera feedback is used to calculate the volume of the clots during rubbing.

C. Closed-Loop Control using Ultrasound Feedback

We use a proportional control input to move the helical robot towards the clot owing to the over-damped characteristic of our system based on its low Reynolds number ($Re = \frac{\rho|\mathbf{U}|L_\mathrm{r}}{\mu} = 0.089$, where ρ and μ are the density and viscosity of the medium, respectively, and L_r is the characteristic length of the robot). The robot position (x_r) is detected using the ultrasound system (Fig. 5) and used to calculate the control input

$$u_1 = k_1\left(x_\mathrm{c} - x_\mathrm{r}\right), \tag{4}$$

where u_1 is the control input to the first rotating dipole field and x_c is the position of the edge of the clot from the side of the helical robot and represents the reference position.

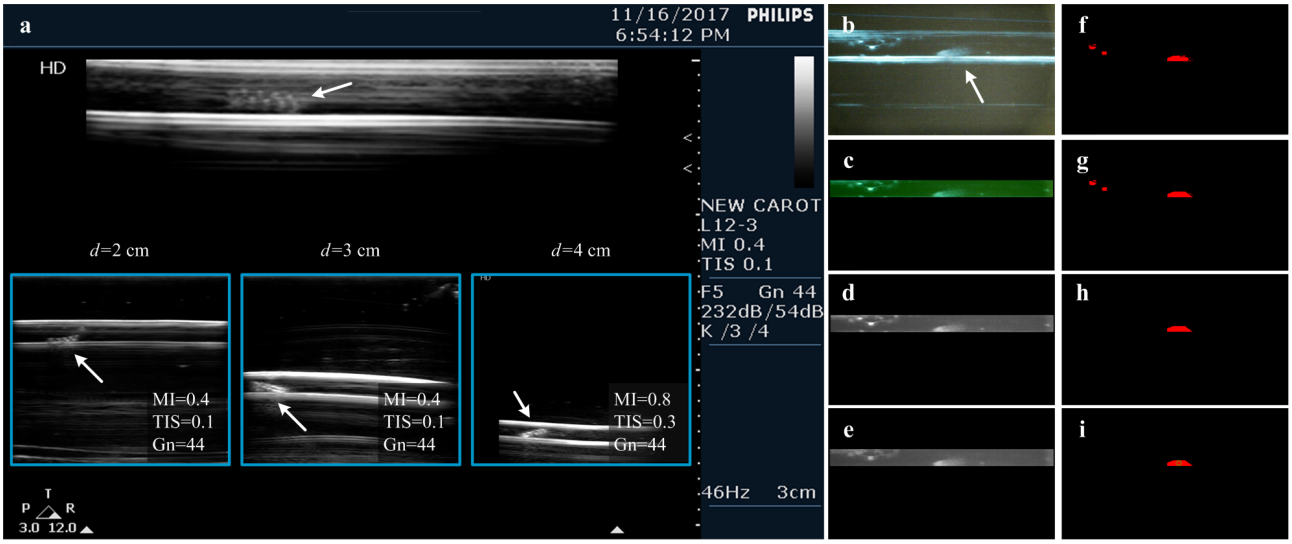

Fig. 5. On-line localization of the helical robot (white arrow) is conducted using ultrasound feedback. Parameters: Thermal index score (TIS) 0.2, mechanical index (MI) 0.9, gain settings (Gn) 43, frequency 3-12 MHz, and depth 1 cm (depth of the catheter segment from the transducer). The insets show representative localization trials at depths of 2 cm, 3 cm, and 4 cm. (a) The catheter segment is contained inside gelatin container and the robot is localized. (b) Image acquisition is done using motion mode. (c) Color subtraction: The RGB color is transformed into luminance Y [21]. (d) Color plane extraction: Extracting green plane (luminance component Y) from RGB components. (e) Gray morphology - *proper opening*: Erosion followed by dilation are implemented for noise removal. (f) Thresholding: A threshold is set to remove the background. (g) Convex hull: The shape of the robot is detected by constructing a convex polygon. (h) and (i) Removal of objects and robot detection: Objects smaller than a specified number of pixels are removed and the robot is localized.

Further, k_1 is a positive proportional gain. This control input is supplied to the first DC motor of the rotating dipole fields as follows:

$$\frac{\mathrm{d}}{\mathrm{d}t}\begin{pmatrix}\omega_i\\ I_i\end{pmatrix} = \underbrace{\begin{pmatrix}-\frac{b}{J} & \frac{k}{J}\\ -\frac{k}{L} & -\frac{R}{L}\end{pmatrix}}_{\mathbf{A}}\begin{pmatrix}\omega_i\\ I_i\end{pmatrix} + \begin{pmatrix}0\\ \frac{1}{L}\end{pmatrix} u_i \text{ for } i = 1, 2, \tag{5}$$

where ω_i and I_i are the angular velocity and input current of the ith DC motor, respectively. Further, b, J, and k are the motor viscous friction constant, moment of inertia of the rotating dipole field and the rotor of the motor, and torque constant, respectively. L and R are the electric inductance and resistance of the motor, respectively. To ensure that the second rotating dipole field is synchronized with the first, we calculate u_2 based on the angular positions of the two motors

$$u_2 = k_2\left(\theta_1 - \theta_2\right) + k_3\left(\omega_1 - \omega_2\right), \tag{6}$$

where k_2 and k_3 are the proportional and derivative positive gains, respectively. Control law (4) provides zero output for zero position tracking error. Therefore, the angular velocity of the rotating dipole fields decreases as the helical robot approaches the reference position. The angular velocity of the rotating dipole fields will ultimately be zero since $\mathbf{A}$ is a Hurwitz matrix. The low Reynolds number characteristic and the control input (4) enable the helical robot to approach the reference position without overshoot. The angular velocity of the rotating dipole fields is the output of the state-space equation (5). This angular velocity is equal to that of the helical robot below its step-out frequency in the absence of interaction with the clot and contact with the channel wall. Therefore, the angular velocity of the motors decrease as the input to the state-space representation (5) decreases with error, and the linear velocity of the robot decreases as it approaches the reference position.

Fig. 6(a) shows a representative closed-loop motion control trial of a helical robot towards a reference position (red dashed line). The robot achieves helical propulsion in PBS at average speed of 2.4 mm/s, and is positioned at the reference position with maximum error of 0.2 mm in the steady-state. We conduct 30 closed-loop control trials and calculate the control characteristics, as shown in Fig. 6(b). The average rise-time and maximum steady-state error are 4 ± 0.2 seconds and 2.15 mm, respectively. The average steady-state error of all trials is 0.84 ± 0.41 mm (n=30). Although the control input (4) achieves stable positioning of the helical robot, it is essential to design more intelligent control strategies and observers based on the physiological conditions of the clots and the technological constraints of the ultrasound system to enhance the robustness and accuracy of the motion control system [20]. *Please refer to the accompanying video.*

D. Mechanical Rubbing of Blood Clots

Closed-loop motion control of the helical robot is followed by mechanical rubbing of the clots. Rubbing is achieved against flow rate of 10 ml/hr. This flow is devised based on the infusion rates of anticoagulation agents. We allow the helical robot to rotate at $\omega = 35$ Hz during the mechanical rubbing. Mechanical rubbing is not efficient below and above this frequency owing to the relatively large drag force due to the induced flow rate and the increased damping at relatively high frequency, respectively. Once the helical robot approaches the clot using control law (4), the dipole fields rotate at $\omega = 35$ Hz and we calculate the size of the

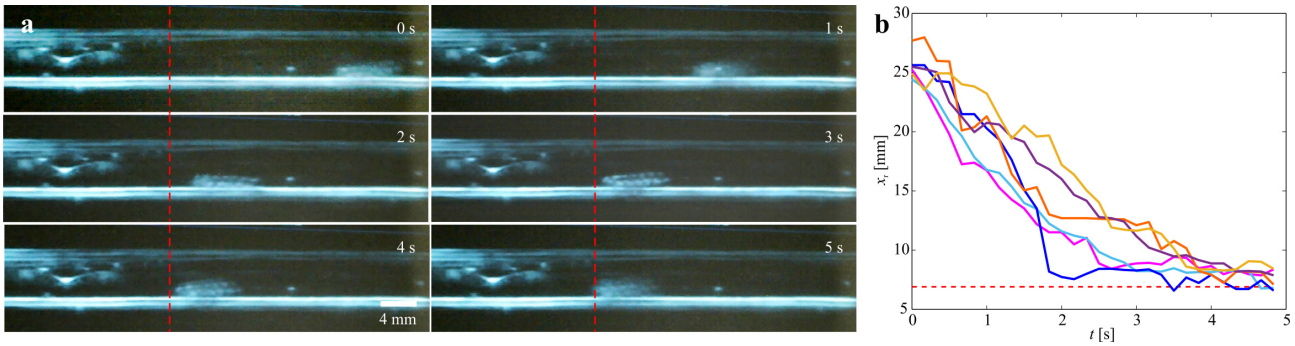

Fig. 6. Closed-loop control of a 4-mm-long helical robot is achieved using ultrasound guidance and under the influence of two rotating dipole fields. (a) The robot swims in phosphate buffered saline inside a catheter segment with inner diameter of 4 mm. The catheter segment is contained inside gelatin container and the ultrasound probe is mounted on its surface. The distance between the probe and the catheter segment is 10 mm. (b) The average speed of the robot is 5.32 ± 1.17 μm/s and the average and maximum steady-state errors are 0.84 ± 0.41 mm and 2.15 mm, respectively. *Please refer to the accompanying video.*

clot using the two cameras shown in Fig. 4. The volume of the clot (v) is determined and used to calculate the nondimensional ratio (v/v_0), where v_0 is the initial volume of the clot, as shown in Fig. 7. We observe that the tip of the helical robot penetrates the clot with an average depth of 0.329 ± 0.46 mm ($n = 6$), whereas our simulation results (Fig. 3(b)) predict penetration of 0.4 mm after 40 minutes of mechanical rubbing. The depth of penetration of the tip of the helical robot is measured based on the overall length of the robot during rubbing since the tip is not visible by the camera feedback. While the predicted penetration depth of the helical robot agrees with our experiment, the helical trajectory inside the clot is not observed experimentally due to the relatively low numbers of frames captured per second (15 frames-per-second) provided by our cameras. In addition, the tip of the robot becomes invisible after a few minutes of interaction with the clot. Therefore, the behaviour predicted by our RFT-based hydrodynamic model is not validated experimentally through visual feedback. However, the difference between the measured and calculated penetration depth shows agreement between experiments and theoretical prediction of our model.

Our ultimate goal is to achieve *in vivo* clearing of blood clots. Therefore, the interaction between the helical robot and the clot is tested at room and body temperatures (25°C and 37°C). Although our rheology test (Fig. 2(b)) indicates that there exist a slight difference in the shear modulus of blood clots at 25°C and 37°C, we calculate the removal rate of the clot at each temperature to study its influence. At 25°C and 37°C, mechanical rubbing achieves average removal rate of -0.614 ± 0.303 mm^3/min ($n = 6$) and -0.482 ± 0.23 mm^3/min ($n = 6$), respectively. Our hydrodynamic model predicts removal rate of -0.5992 mm^3/min. This removal rate is in agreement with the trials conducted at temperature of 25°C. We attribute this observation to the characterized parameters entered to the model. Characterization of the clots is done at 25°C. Therefore, mechanical rubbing results at 25°C are in agreement with our theoretical prediction. This experimental result also show that mechanical rubbing of blood clots remains efficient under 37°C. Therefore, our *in vitro* model (Fig. 4) mimics essential *in vivo* conditions. *Please refer to the accompanying video.*

The interaction between the rotating tip of the helical robot and the blood clot enables RBCs and platelets to break free from its fibrin network. To validate this observation, we use a hemocytometer to measure the concentration of RBCs and platelets in the mixture past the clot and the robot. This mixture is collected every 5 minutes and the concentration of RBCs and platelets is calculated, as shown in Fig. 8. First, concentration of RBCs and platelets is calculated in the absence of mechanical rubbing for 40 minutes against flow rate of 10 ml/hr (Fig. 8(a)). After 5 minutes, the cell count is $113 \pm 16.7 \times 10^4$ cell/ml ($n = 4$), and we observe that the cell count converges to less than 3×10^4 cell/ml after 15 minutes. After 40 minutes the cell count is $2 \pm 1.41 \times 10^4$ cell/ml. The cell count is relatively high in the first 5 minutes owing to the forces exerted on the blood clot samples during insertion. After this transient response, the number of cells is drastically decreased and cells are trapped within the fibrin fibers of the clot. Second, the concentration of the RBCs and platelets is measured during rubbing at $\omega = 35$ Hz against the same flow rate (Fig. 8(b)). In contrast to the previous idle test, the cell count during mechanical rubbing with the helical robot indicates that RBCs and platelets break free from the fibrin network of the clot throughout the whole rubbing test. After 5 minutes of mechanical rubbing, the count of RBCs and platelets is $211 \pm 131.6 \times 10^4$ cell/ml ($n = 4$), and converges to approximately 120×10^4 cell/ml ($n = 4$) throughout the rubbing trials, as shown in Fig. 8(c). Finally, after 40 minutes of mechanical rubbing, the cell count is calculated to be $46 \pm 10.9 \times 10^4$ cell/ml ($n = 4$). The continuous interaction between the helical robot and the clot enables more RBCs and platelets to break free from the fibrin network with time. Therefore, effectiveness of mechanical rubbing is demonstrated by the removal rate of clots (Fig. 7) and the blood cells count past the clot (Fig. 8). The measured volume ratio (v/v_0) and the total cell count indicate that 40 minutes of rubbing result in the removal of 24.56 ± 12.1 mm^3 and 7.49 ± 1.86 mm^3, respectively. We attribute the difference between these techniques to the

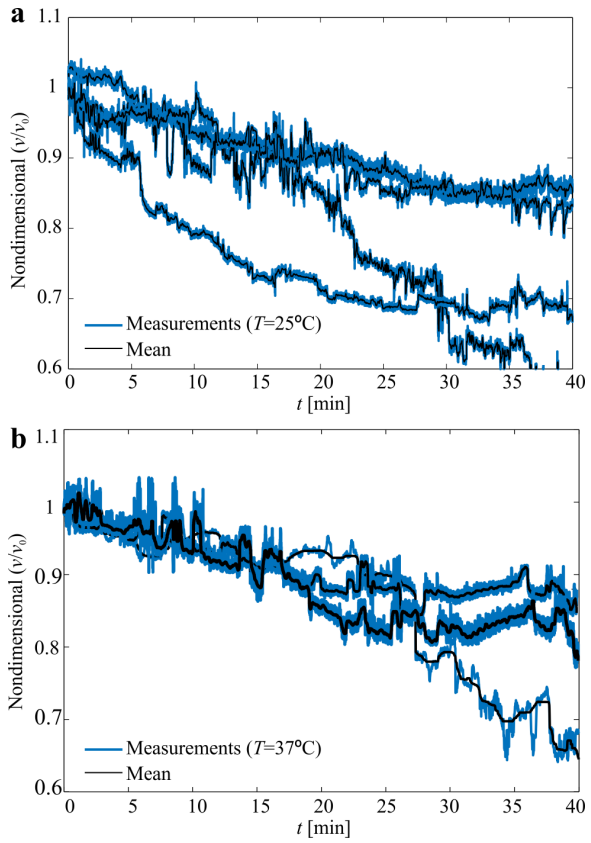

Fig. 7. Influence of the mechanical rubbing on the removal rate of clots is characterized at room temperature of 25°C and body temperature of 37°C. 1-hour-old blood clot samples are used during rubbing. (a) Mechanical rubbing achieves removal rate of -0.614 ± 0.303 mm^3/min ($n = 6$) at 25°C. 7.5-mm-long blood clot samples with diameter of 4 mm are used during the rubbing trials with rotating magnetic field at $\omega = 35$ Hz. (b) Mechanical rubbing achieves removal rate of -0.482 ± 0.23 mm^3/min ($n = 6$) at 37°C. *Please refer to the accompanying video.*

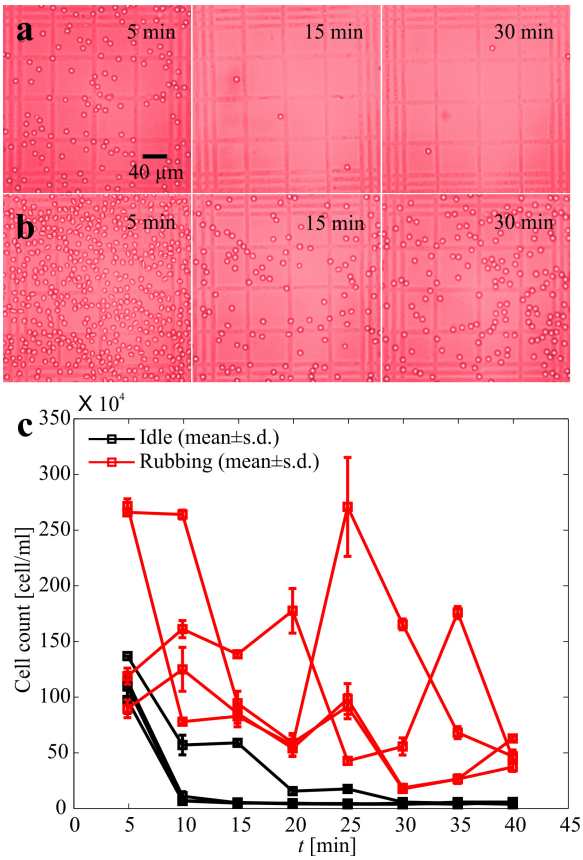

Fig. 8. Number of red blood cells (RBCs) and platelets is analyzed to study the influence of rubbing on blood clots. Interaction between the tip of the helical robot and the fibrin network of the clot allows RBCs and platelets to break free. Mixture past the clot (1-hour-old clot samples) and the helical robot is collected every 5 minutes and analyzed using a hemocytometer. Averages and standard deviations are calculated for 4 idle and rubbing rials. (a) RBCs and platelets are counted for input flow of 10 ml/hr without rubbing. (b) RBCs and platelets are counted during mechanical rubbing at $\omega = 35$ Hz, and against flow rate of 10 ml/hr. (c) The cell count indicates that rubbing allows more RBCs and platelets to break free from the fibrin network with time.

dissolution of fibrin. The fibrin fibers have average diameter of approximately 328 nm (Fig. 2(a)). These fibers are not taken into consideration during cell count, and thus the measured volume using visual feedback provide relatively larger rate compared to cell count.

IV. Discussions

The formation of blood clots starts with the activation and aggregation of tiny blood cells (platelets) followed by the activation of blood coagulation factors generating strands of fibrin surrounding the platelets. More platelets and red blood cells are then entrapped inside the fibrin network. The mechanical rubbing of the blood clot enables the entrapped blood cells to break free from its fibrin network as evidenced by the variation in the cell count in the solution past the clot throughout the experiments. However, these exist several challenges that have to be overcome to translate this technique into *in vivo* experiments. The echogenicity of fresh clots (approximately 1-hour-old) has to be enhanced to enable localization. Our ultimate goal is to clear clots *in vivo*, thus localization of the helical robot and the clots in the blood vessels is crucial. Under the current experimental conditions, the clots could not be clearly visualized. This observation is in agreement with previously reported properties of fresh blood clots being isoechoic to flowing blood and become more echogenic with increasing age [22]. It is also essential to coat the helical robots with biocompatible or drug-delivery coatings (gold-coated vascular stents yield less macroscopic and histopathological changes in vessels than those coated with silver, copper, or silicon [23]) to inhibit coagulation around the robot and prevent releasing ions that will lead to inflammatory reactions.

Our cell count analysis (Fig. 8) indicates the presence of RBCs and platelets only in the mixture past the helical robot. Small fragments of blood clots are not observed in any of our mechanical rubbing trials. Therefore, the interaction between the tip of the helical robot and the fibrin fibers of the clot does not lead to disintegration of smaller clot fragments in our trials. However, clot-to-clot variability in properties and shape during formation could possibly result in fragments upon interaction with the helical robot. Formation of these

small clot fragments could cause significant problems if they are carried with the blood flow to a smaller vessel. Although we do not observe formation of clot fragments in our *in vitro* experimental results, this risk can be mitigated by the integration of chemical lysis (with relatively small dose) with mechanical rubbing.

V. Conclusions and Future Work

We demonstrate closed-loop motion control of helical robots towards blood clots and mechanical rubbing under ultrasound guidance. First, we move the helical robot controllably towards the clot at an average speed of 5.32 ± 1.17 μm/s using a proportional control input without overshoot. This control input is designed using ultrasound feedback and enables the helical robot to achieve average and maximum steady-state errors of 0.84 ± 0.41 mm and 2.15 mm, respectively, and average settling time of 4.5 ± 0.1 seconds. The closed-loop motion control of the helical robot is followed by mechanical rubbing to decrease the size of the clots. We show that mechanical rubbing at $\omega = 35$ Hz achieves average removal rate of -0.614 ± 0.303 mm^3/min ($n = 6$) and -0.482 ± 0.23 mm^3/min ($n = 6$) at temperature of 25°C and 37°C, respectively. We also validate the effectiveness of the mechanical rubbing in tearing the fibrin network of the clots by measuring the average number of RBCs and platelets past the clot. The helical robot achieves cell count (RBCs and platelets) of $832.91 \pm 206.6 \times 10^4$ cell/ml ($n = 4$), whereas the cell count in the absence of rubbing is $162.75 \pm 81.25 \times 10^4$ cell/ml ($n = 4$).

As part of future studies, we will increase the blood clots echogenicity to enable position and size detection using ultrasound feedback. The clots will be functionalized using echogenic liposome compositions to enhance the ultrasound detection. We will also study the influence of rubbing in combination with chemical lysis at different doses of a fibrinolytic agent. The comparative study between mechanical rubbing, rubbing in combination with different percentages of fibrinolytic agent, and pure chemical lysis is essential to optimize the integration between mechanical rubbing and chemical lysis. Our experimental results are conduced against flow rate of 10 ml/hr. This flow rate is greater than blood flow in small arteriole, capillaries, and venule only. Therefore, it is essential to modify our system to enable mechanical rubbing against greater flow rates comparable to medium arteries and veins.

References

[1] R. A. Freitas Jr., "Nanotechnology, nanomedicine and nanosurgery," *International Journal of Surgery*, vol. 3, no. 4, pp. 243-246, April 2005.

[2] M. Vonthron, V. Lalande, G. Bringout, C. Tremblay, and S. Martel, "A MRI-based integrated platform for the navigation of microdevices and microrobots," in *Proceedings of the IEEE J International Conference on Intelligent Robots and Systems (IROS)*, pp. 1285–1290, San Francisco, USA, September 2011.

[3] A. Servant, F. Qiu, M. Mazza, K. Kostarelos, and B. J. Nelson, "Controlled in vivo swimming of a swarm of bacteria-like microrobotic flagella," *Advanced Materials*, vol. 27, no. 19, pp. 2981-2988, April 2015.

[4] O. Felfoul, M. Mohammadi, S. Taherkhani, D. de Lanauze, Y. Z. Xu, D. Loghin, S. Essa, S. Jancik, D. Houle, M. Lafleur, L. Gaboury, M. Tabrizian, N. Kaou, M. Atkin, T. Vuong, G. Batist, N. Beauchemin, D. Radzioch, and S. Martel, "Magneto-aerotactic bacteria deliver drug-containing nanoliposomes to tumour hypoxic regions," *Nature Nanotechnology*, August 2016

[5] S. K. Srivastava, M. M.-Sánchez, B. Koch, and O. G. Schmidt, "Medibots: dual-action biogenic microdaggers for single-cell surgery and drug release," *Advanced Materials*, vol. 28, no. 5, pp. 832–837, November 2015.

[6] B. E.-Fernández de Ávila, P. Angsantikul, J. Li, M. A. Lopez-Ramirez, D. E. Ramrez-Herrera, S. Thamphiwatana, C. Chen, J. Delezuk, R. Samakapiruk, V. Ramez, L. Zhang, and J. Wang, "Micromotor-enabled active drug delivery for in vivo treatment of stomach infection," *Nature Communications*, vol. 8, no. 272, August 2017.

[7] A. Ghosh and P. Fischer, "Controlled propulsion of artificial magnetic nanostructured propellers," *Nano Letters*, vol. 9, pp. 2243-2245, June 2009.

[8] I. S. M. Khalil, A. F. Tabak, A. Klingner, and M. Sitti, "Magnetic propulsion of robotic sperms at low-Reynolds number," *Applied Physics Letters*, vol. 109 (033701), July 2016.

[9] W. F. Paxton, K. C. Kistler, C. C. Olmeda, A. Sen, S. K. St. Angelo, Y. Cao, T. E. Mallouk, P. E. Lammert, and V. H. Crespi, "Catalytic nanomotors: autonomous movement of striped nanorods," *Journal of the American Chemical Society*, vol. 126, no. 41, pp. 13424–13431, September 2004.

[10] W. Wang, L. A. Castro, M. Hoyos, T. E. Mallouk, "Autonomous motion of metallic microrods propelled by ultrasound," *ACS Nano*, vol. 6, no. 7, pp. 6122–6132, May 2012,

[11] P. Calvo-Marzal, S. Sattayasamitsathit, S. Balasubramanian, J. R. Windmiller, C. Dao, J. Wang, "Propulsion of nanowire diodes," *Chemical Communications*, vol. 46, no. 10, pp. 1623–1624, February 2010.

[12] M. Pumera, "Electrochemically powered self-propelled electrophoretic nanosubmarines," *Nanoscale*, vol. 2, no. 9, pp. 1643–1649, May 2010.

[13] K. K. Coti, M. E. Belowich, M. Liong, M. W. Ambrogio, Y. A. Lau, H. A. Khatib, J. I. Zink, N. M. Khashab, and J. F. Stoddart, "Mechanised nanoparticles for drug delivery," *Nanoscale*, vol. 1, no. 16, pp. 16-39, September 2009.

[14] S. Campuzano, D. Kagan, J. Orozco, and J. Wang, "Motion-Driven sensing and biosensing using electrochemically propelled nanomotors," *Analyst*, 136, 4621–4630, September 2011.

[15] J. Liu, J. Wen, Z. Zhang, H. Liu, and Y. Sun, "Voyage inside the cell: microsystems and nanoengineering for intracellular measurement and manipulation," *Microsystems & Nanoengineering*, vol. 1, no. 15020, September 2015.

[16] I. S. M. Khalil, A. F. Tabak, K. Sadek, D. Mahdy, N. Hamdi, and M. Sitti, "Rubbing against blood clots using helical robots: modeling and in vitro experimental validation," *IEEE Robotics & Automation Letters*, vol. 2, no. 2, pp. 927-934, April 2017.

[17] A. Hoffmann and H. Gill, "Diastolic timed vibro-percussion at 50 Hz delivered across a chest wall sized meat barrier enhances clot dissolution and remotely administered streptokinase effectiveness in an in-vitro model of acute coronary thrombosis," *Thrombosis Journal*, vol. 10, no. 23, pp. 1–16, November 2012.

[18] D. B. Cines, T. Lebedeva, C. Nagaswami, V. Hayes, W. Massefski, R. I. Litvinov, L. Rauova, T. J. Lowery, and J. W. Weisel, "Clot contraction: compression of erythrocytes into tightly packed polyhedra and redistribution of platelets and fibrin," *Blood*, vol. 123, no. 10, pp. 1596-1603, March 2014.

[19] A. Hosney, J. Abdalla, I. S. Amin, N. Hamdi, and I. S. M. Khalil, "*In vitro* validation of clearing clogged vessels using microrobots," in *Proceedings of the IEEE RAS/EMBS International Conference on Biomedical Robotics and Biomechatronics (BioRob)*, pp. 272-277, Singapore, June 2016.

[20] L. Sadelli, M. Fruchard, and A. Ferreira, "2D observer-based control of a vascular microrobot," *IEEE Transactions on Automatic Control*, vol. 62, no. 5, pp. 2194–2206, May 2017.

[21] K. N. Plataniotis and A. N. Venetsanopoulos, "Color image processing and applications," *Springer-Verlag*, New York, NY, USA March 2000.

[22] T. S. Wu, "Ultrasound: Part 2, An issue of critical care clinics," *Elsevier Health Sciences*, vol. 30, no. 2, pp. 169, March 2014.

[23] N. Tanigawa, S. Sawada, and M. Kobayashi, "Reaction of the aortic wall to six metallic stent materials," *Academic Radiology*, vol. 2, no. 5, pp. 379–384, May 1995.